transfer is enhanced by the additional nitro group.

Enhancement of β has been realized in 2',4'-dimethoxy-4-nitrostilbene, in which the donor-group dipole moment is small. This is consistent with the effect of mutual orientation of μ and β_μ. This result and the fact that the actual nonresonant redistribution of electron density by the applied field is small suggest that the system is not at saturation polarization. Therefore, it is likely that the lower β_μ results from a redirection of the dipole moment. The usable nonlinearity in electric-field aligned structures such as poled polymeric systems is represented by β_μ.[20] Since $\mu\cdot\beta$ for the dinitrostilbenes is comparable to those for the nitrostilbenes, the former exhibit no appreciable improvement for poled polymer applications. It is possible that some tensor components of β are enhanced upon multiple substitution. These enhancements may be manifested in single crystals.

Powder SHG Efficiencies. Even if the molecular hyperpolarizabilities of the dinitrostilbene compounds are smaller than those for the nitrostilbenes, on an absolute scale they are nonetheless large. This strongly implies that the small SHG efficiencies observed are a consequence of centrosymmetric or nearly centrosymmetric packing of the chromophores in the crystal lattice. Roughly 75% of all organic molecules crystallize in centrosymmetric space groups leading to materials with vanishing $\chi^{(2)}$. Since dipolar interactions provide a strong driving force for centrosymmetric crystallization, it is expected that the relatively large dipole moments of the dinitrostilbenes contribute to the unfavorable packing. Even for 4'-[2-(hydroxymethyl)pyrrolidinyl]-2,4-dinitrostilbene, the relatively small SHG efficiency indicates that although the compound crystallizes in a noncentrosymmetric space group, the alignment of the molecules in the lattice must be far from the ideal geometry for second harmonic generation. This is in contrast to (nitrophenyl)prolinol (NPP), a yellow compound with an SHG efficiency (SH at 532 nm) about 150 times that of urea.[14]

(20) Singer, K. D.; Sohn, J. E. Lalama, S. J. *Appl. Phys. Lett.* **1986**, *49*, 248.

Acknowledgment. The research described in this paper was performed by the Jet Propulsion Laboratory, California Institute of Technology, as part of its Center for Space Microelectronics Technology, which is supported by the Strategic Defense Initiative Organization, Innovative Science and Technology Office through an agreement with the National Aeronautics and Space Administration (NASA). S.R.M. thanks Professor Robert Grubbs for access to synthetic facilities at Caltech and the National Research Council and NASA for a National Research Council Resident Research Associateship at the Jet Propulsion Laboratory.

Registry No. (*E*)-2,4-$(O_2N)_2C_6H_3CH{=}CHC_6H_4OMe$-*o*, 129540-39-2; (*E*)-2,4-$(O_2N)_2C_6H_3CH{=}CHC_6H_4OMe$-*p*, 129540-40-5; (*E*)-2,4-$(O_2N)_2C_6H_3CH{=}CHC_6H_4NMe_2$-*p*, 61599-67-5; (*E,E*)-2,4-$(O_2N)_2C_6H_3CH{=}CHCH{=}CHC_6H_4NMe_2$-*p*, 129540-43-8; (*E*)-2,4-$(O_2N)_2C_6H_3CH{=}CH(C_5H_4FeC_5H_5)$, 129540-46-1; *o*-$MeOC_6H_4CHO$, 135-02-4; *p*-$MeOC_6H_4CHO$, 123-11-5; 2,4-$(CH_3O)_2C_6H_3CHO$, 613-45-6; 4-$(CH_3)_2NC_6H_4CHO$, 100-10-7; (*E*)-4-$(CH_3)_2NC_6H_4CH{=}CHCHO$, 20432-35-3; $C_5H_5FeC_5H_4CHO$, 12093-10-6; (*E*)-1,2-bis(2,4-dimethoxyphenyl)ethylene, 129540-41-6; (*E*)-1-(2,4-dinitrophenyl)-2-(1-pyrenyl)ethylene, 129540-42-7; 4'-[2-(hydroxymethyl)pyrrolidinyl]-2,4-dinitrostilbene, 129540-44-9; 1-pyrenecarboxaldehyde, 3029-19-4; 4'-[2-(hydroxymethyl)pyrrolidinyl]benzaldehyde, 129540-45-0; 2,4-dinitrotoluene, 121-14-2.

Solid-Phase Equilibria for Metal–Silicon–Oxygen Ternary Systems. 1. Mg, Ca, Sr, and Ba

Haojie Yuan and R. Stanley Williams*

Department of Chemistry and Biochemistry and Solid State Science Center, University of California, Los Angeles, Los Angeles, California 90024-1569

Received December 20, 1989

Ternary-phase diagrams for systems of the type M–Si–O, where M = Mg, Ca, Sr, and Ba, have been derived. These phase diagrams can be used to understand experimental results reported in the literature for thin-film chemical reactions of SrO on Si and provide guides in designing stable structures that involve different materials in intimate contact. These particular phase diagrams are especially relevant for investigating the chemical stability of interfaces between SiO_2 and the oxide superconductors.

Introduction

Chemical reactions that occur at the interfaces separating different solids are scientifically interesting and technologically important. Many studies have shown that one of the first steps in understanding and controlling interfacial chemistry is to map the bulk-phase diagram containing the elements of interest.[1-6] These phase diagrams can be used to predict the occurrence of reaction products or, conversely, the stability of the phases present at the interfaces between different materials. Hence, bulk-phase diagrams can provide guides in designing thin-film structures and in selecting candidate materials to form chemically stable interfaces.

In this work, we derived phase diagrams for systems of the type M–Si–O, where M = Mg, Ca, Sr, and Ba. These

* To whom correspondence should be addressed at the Department of Chemistry and Biochemistry.

(1) Schwartz, G. P.; Gaultieri, G. J.; Griffiths, J. E.; Thurmond, C. D.; Schwartz, B. *J. Electrochem. Soc.* **1980**, *127*, 2488.
(2) Thurmond, C. D.; Schwartz, G. P.; Kammlott, G. W.; Schwartz, B. *J. Electrochem. Soc.* **1980**, *127*, 1366.
(3) Schwartz, G. P. *Thin Solid Films* **1983**, *103*, 3.
(4) Beyers, R. *Mater. Res. Soc. Proc.* **1985**, *47*, 143.
(5) Tsai, C. T.; Williams, R. S. *J. Mater. Res.* **1986**, *1*(2), 352.
(6) Pugh, J. H.; Williams, R. S. *J. Mater. Res.* **1986**, *1*(2), 343.

0897-4756/90/2802-0695$02.50/0

Table I. Enthalpies of Formation (kJ/mol) of the Phases in the Mg–Si–O System at 298 K and 1 atm

	references	estimated
SiO_2	−910.2 ± 3.3[a]	
	−910.72 (α quartz)[b]	
	−909.24 (α cristobalite)[b]	
	−908.24 (α tridymite)[b]	
	−903.28 (α amo)[b]	
	−910.94 (α quartz)[d,i]	
	−909.48 (α cristobalite)[d]	
	−909.06 (α tridymite)[d]	
	−903.5 (amo)[d]	
	−871.3 (α quartz)[e]	
	−864.2 (β cristobalite)[e]	
MgO	−601.1 ± 0.8[a]	
	−601.56[b]	
	−597.83 (micro)[b]	
	−601.70[d,i]	
	−597.98 (micro)[d]	
	−601.2 ± 0.63[h]	
MgO_2	−628.4[b,i]	
Mg_2Si	−79.1 ± 5.0[a]	
	−77.8[b]	
	−77.4 ± 6.3[c]	
	−77.8[d,i]	
	−77.8[f]	
	−42.7 to −89.2[g]	
Mg_2SiO_4	−2175.1 ± 2.1[a]	
	−2173.5[b]	
	−2174.0[d,i]	
$MgSiO_3$	−1547.7 ± 2.9[a]	−1550
	−1548.63[b]	
	−1549.00[d,i]	
	−1548.93 ± 4.2[h]	

[a] Data from ref 8. [b] Data from ref 9. [c] Data from 10. [d] Data from ref 11. [e] Data from ref 12. [f] Data from ref 19. [g] Data from ref 20. [h] Data from ref 23. [i] Data used for the calculations and estimations in this paper.

phase diagrams are important for understanding how elemental Si interacts with the group II metal oxides (MgO, CaO, SrO, and BaO), how the group II metals interact with SiO_2, and how the oxide superconductors interact with SiO_2 and Si. We will describe how to determine such phase diagrams, present the ternary diagrams for the M–Si–O systems, and discuss the use of these phase diagrams for understanding interfacial chemistry.

Determination of Ternary Phase Diagrams

The procedures required for mapping out ternary phase diagrams have been discussed in detail by several authors.[2,4,5] The convention in this paper follows that established by Thurmond et al.[2] for representing the solidus portion of a ternary diagram involving oxygen as one of the components; the partial pressure of oxygen in the system is chosen to be 1 atm. Isothermal sections of the diagrams are represented as equilateral triangles with each apex representing a system containing only a single element, in this case oxygen, silicon, or a group II metal. The sides of the triangle present the compounds that can exist in each of the possible binary systems. The interior of the diagram is subdivided by tie lines into smaller triangles that represent the regions of three-phase equilibrium. The tie lines can be determined by simple calculations if the Gibbs energy of formation (ΔG_f) of all the phases in the systems are known.

Unfortunately, the thermochemical data base has large gaps and many uncertainties, so in practice, phase diagrams have been constructed with the use of several approximations supplemented by experimental determinations of phase stability.[1-6] The major assumption often made is that the entropic contribution to a solid-state reaction is negligible and that the phase stabilities may

Table II. Enthalpies of Formation (kJ/mol) of the Phases in the Ca–Si–O System at 298 K and 1 atm

	references	estimated
CaO	−634.1 ± 1.7[a]	
	−634.94[b]	
	−635.09[d,i]	
	−635.09 ± 0.88[h]	
CaO_2	−658.8 ± 2.1[a]	
	−652.5[b]	
	−652.7[d,i]	
Ca_2Si	−209.1 ± 12.5[a]	−196.2
	−209 ± 13[c]	
	−209[d,i]	
	−209 ± 13[f]	
Ca_5Si_3		−558
CaSi	−150.6 ± 8.4[a]	
	−151 ± 8[c]	
	−151[d,i]	
	−151 ± 8[f]	
$CaSi_2$	−150.6 ± 12.5[a]	−196.2
	−151 ± 8[c]	
	−151[d,i]	
	−151 ± 13[f]	
Ca_3SiO_5	−2925.6 ± 6.3[a]	−2972
	−2928.5[b]	
	−2929.2[d,i]	
Ca_2SiO_4	−2315.3 ± 8.4[a]	
	−2306.9 (β)[b]	
	−2317.7 (γ)[b]	
	−2307.5 (β)[d,i]	
	−2317.9 (γ)[d]	
$Ca_8Si_5O_{18}$		−10179
$Ca_3Si_2O_7$	−3960.0[b]	−3935
	−3961.0[d,i]	
$CaSiO_3$	−1633.4 ± 1.3[a]	−1624
	−1634.54[b]	
	−1628.0[b]	
	−1600.62[b]	
	−1634.94 (wollastonite)[d,i]	
	−1628.4 (pseudowollastonite)[d]	
$CaSi_2O_5$		−2546

[a] Data from ref 8. [b] Data from ref 9. [c] Data from ref 10. [d] Data from ref 11. [f] Data from ref 19. [h] Data from ref 23. [i] Data used for the calculations and estimations in this paper.

be determined from the enthalpies of formation (ΔH_f). Another assumption used here is that the phases have a negligible solid solubility in one another, so that the tie lines are straight and phase boundaries are abrupt. Finally, if no ΔH_f data exist for a particular phase, it can be estimated by interpolation procedures from known phases. For this work, the missing data were estimated by using the method in ref 7. For the silicates, the reference states used for the estimates were the solid oxides SiO_2 and MO.

For the case of the M–Si–O systems studied here, many references have been consulted to find what phases exist in each ternary system.[8-19] There have been several de-

(7) Pugh, J. H. Thermochemical Studies of Transition Metal/III-V compound-semiconductor Interfaces. Master's Thesis, UCLA, 1986; p 113.
(8) Kubaschewski, O.; Alcock, C. B. *Metallurgical ThermoChemistry*, 5th ed.; Pergamon Press: Oxford, 1979; p 268.
(9) *CRC Handbook of Chemistry and Physics*, 68th ed.; CRC Press: Boca Raton, FL, 1987.
(10) Berezhnoi, A. S. *Silicon and Its Binary Systems*; Consultants Bureau: New York, 1979.
(11) Wagman, D. D.; Evans, W. H.; Parker, V. B.; Schumm, R. H.; Halow, I.; Bailey, S. M.; Churney, K. L.; Nuttall, R. L. *J. Phys. Chem. Ref. Data* **1982**, *11*, Suppl. No. 2.
(12) Glushkova, V. B. *Zh. Neorg. Khim.* (*J. Inorg. Chem. USSR*) **1957**, 2, 2438.
(13) Toropov, N. A.; Barzakovskii, V. P.; Lapin, V. V.; Kurtseva, N. N. *Handbook of Phase Diagrams of Silicate Systems*, Israel Program for Scientific Translations: Jerusalem, 1972; Vols. 1, 2.
(14) Hanson, M. *Constitution of Binary Alloys*; McGraw-Hill: New York, 1969.

Table III. Enthalpies of Formation (kJ/mol) of the Phases in the Sr–Si–O System at 298 K and 1 atm

	references	estimated
SrO	−591.9 ± 3.8[a]	
	−591.9[b]	
	−592.0[d,j]	
	−590.2[e]	
	−592.04 ± 3.3[h]	
SrO_2	−633.3 ± 15.1[a]	
	−633.3[b]	
	−633.5[d,j]	
	−642.5[e]	
Sr_2Si	−485[f]	−87.8[j,k]
SrSi	−472.7[c]	−76.4[k]
	−556.4[f]	
	−91.5[i–k]	
Sr_2Si_3		−204.5[j,k]
$SrSi_2$	−616.6[c]	
	−786.6[f]	
	−124.5[i–k]	
Sr_3SiO_5	−2792.2[e,j]	−2945
Sr_2SiO_4	−2303.2 ± 3.3[a]	
	−2304.0[b]	
	−2304.5[d,j]	
	−2194.0[e]	
$SrSiO_3$	−1632.6 ± 2.1[a]	−1632
	−1633.5[b]	
	−1633.9[d,j]	
	−1552.7[e]	

[a] Data from ref 8. [b] Data from ref 9. [c] Data from ref 10. [d] Data from ref 11. [e] Data from ref 12. [f] Data from ref 19. [h] Data from ref 23. [i] Data from ref 21. [j] Data used for the calculations and estimations in this paper. [k] Data for the liquid silicides.

terminations and revisions of the available thermochemical data.[8–12,19–23] The ΔH_f data obtained from refs 8–12 and 19–23 were compared, and it was found that the agreement among the different references for which independent determinations of the same values have been made is very good. Since the data from ref 11 were compiled to form a consistent set, these values have been used whenever possible in the calculations of this paper. Tables I–IV also contain data from refs 9, 10, 12, and 19–23 as well as the estimated enthalpies of formation to fill in the gaps and to show the consistency among the different determinations.

The calculated enthalpy change for a reaction used in determining the position of a tie line in a phase diagram is subject to the following uncertainties: (1) The phase diagrams are for the standard states at 298 K and 1 atm, but the data from ref 11 are for the conditions of 298 K and 0.1 MPa. According to ref 11, this minor difference in pressure will not affect the tabulated data for the solid compounds. (2) The data from ref 11 are characterized by absolute experimental uncertainties of less than 8 kJ, with the relative uncertainties considerably smaller. (3)

Table IV. Enthalpies of Formation (kJ/mol) of the Phases in the Ba–Si–O System at 298 K and 1 atm

	references	estimated
BaO	−553.2 ± 18.8[a]	
	−553.5[d,j]	
	−548.1 ± 2.1[h]	
BaO_2	−634.1 ± 11.7[a]	
	−634.1[b]	
	−634.3[d,j]	
Ba_2Si		−108.5[j,k]
Ba_5Si_3		−316.5[j,k]
BaSi	−757[c]	−94.6[k]
	−837[f]	
	−97.8[i–k]	
Ba_3Si_4		−349.4[j,k]
$BaSi_2$	−153.6[i,j]	−1359
Ba_4SiO_6	−3249.1[e,j]	−3489
Ba_3SiO_5	−2709.7[e,j]	−2904
Ba_2SiO_4	−2286.8 ± 4.2[a]	
	−2287.3[b]	
	−2287.8[d]	
	−2126.2[e]	
$BaSiO_3$	−1622.6 ± 4.2[a]	−1631
	−1623.2[b]	
	−1623.6[d,j]	
	−1573 (amo)[d]	
$Ba_2Si_3O_8$	−4183.8[b]	−4204
	−4184.8[d,j]	
$Ba_5Si_8O_{21}$		−10975
$Ba_3Si_5O_{13}$		−6771
$BaSi_2O_5$	−2547.4[b]	−2566
	−2548.1[d,j]	
$BaSi_4O_9$		−4401

[a] Data from ref 8. [b] Data from ref 9. [c] Data from ref 10. [d] Data from ref 11. [e] Data from ref 12. [f] Data from ref 19. [h] Data from ref 23. [i] Data from ref 22. [j] Data used for the calculations and estimations in this paper. [k] Data for liquid silicides.

The data from the other references, which do not have uncertainties listed, and the estimated data are assumed to have uncertainties comparable to the largest uncertainty values for the tabulated phases, with the notable exception of the silicides.

We used the ΔH_f data from refs 21 and 22 for the Sr silicides and Ba silicides in our calculations. These data are for the liquid Sr silicides and Ba silicides, which were obtained at 1766 and 1723 K, respectively. We believe that the ΔH_f data for the solid Sr silicides and Ba silicides in refs 10 and 19 are improbably high, as Esin et al.[22] have pointed out. By tracing back to the original sources, we found that the values −472.7 and −616.6 kJ/mol for SrSi and $SrSi_2$, respectively, and −757 kJ/mol for BaSi were reported by Wohler and Shuff[24] in 1932. The enthalpies of formation of liquid and solid alloys usually have similar values.[22] The ΔH_f data for the liquid and solid Sr and Ba silicides are listed together in the Tables III and IV, which reveal the major difference between the ΔH_f data for the liquid and solid silicides. On the basis of the above, we have used ΔH_f values interpolated from the known data of the liquid Sr and Ba silicides for our phase diagram calculations.

Some ΔH_f values had to be estimated. We estimated the ΔH_f values for all the silicates. This allowed us to compare the estimated values with the actual values for the compounds for which ΔH_f values are known and thus provide a way to evaluate how accurate the estimated data are. In the Ca–Si–O system, $CaSi_2O_5$ and $Ca_8Si_5O_{18}$ are the compounds for which ΔH_f values used in the phase diagram calculations were estimated. These estimated values probably have relative errors no greater than 1.5%,

(15) Shunk, F. A. *Constitution of Binary Alloys*; McGraw-Hill: New York, 1969; Second Supplement.
(16) Moffatt, W. G. *Binary Phase Diagrams Handbook*; General Electric Co.: Schenectady, NY, 1977.
(17) Villars, P.; Calver, L. D. *Pearson's Handbook of Crystallographic Data for Intermetallic Phases*; American Society for Metals: Metal Park, OH, 1985.
(18) *JCPDS Powder Diffraction File, Inorganic Phases, Alphabetical Index*; Chemical and Mineral Name, 1987.
(19) Samsonov, G. V.; Vinitskii, I. M. *Handbook of Refractory Compounds*; IfI/Plenum Data Co.: New York, 1980.
(20) Nayeb-Hashemi, A. A.; Clark, J. B. *Bull. Alloy Phase Diagrams* **1984**, *5*, 584.
(21) Esin, Yu. O.; Kolesnikpov, S. P.; Baev, V. M.; Valishev, M. G.; Gel'd, P. V.; Zaiko, V. P.; Ryss, M. A. *Zh. Fiz. Khim.* **1979**, *53*, 1624.
(22) Esin, Yu. O.; Sandakov, V. M.; Gel'd, P. V.; Ryss, M. A.; Golev, A. K.; Zaiko, V. P. *Zh. Prikl. Khim.* **1973**, *46*, 2402.
(23) *JANAF Thermochemical Tables*, 3rd ed.; American Chemical Society and American Institute of Physics: Washington, DC, 1985.
(24) Wohler, L.; Shuff, W. *Z. Anorg. Chem.* **1932**, *209*, 33.

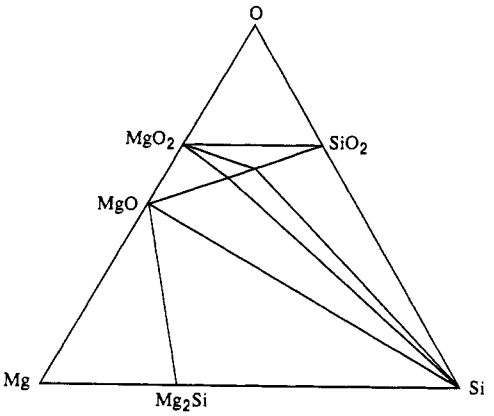

Figure 1. Mg–Si–O phase diagram at 298 K and 1 atm. Compounds from left to right on the $MgO–SiO_2$ line are Mg_2SiO_4 and $MgSiO_3$.

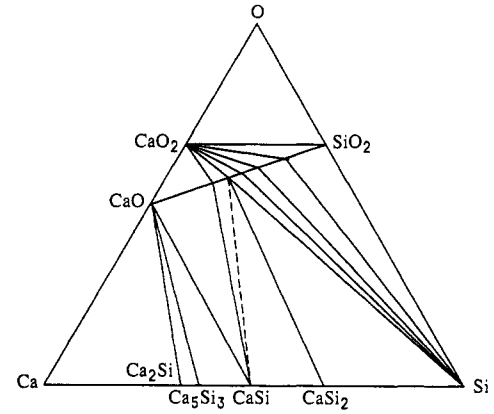

Figure 2. Ca–Si–O phase diagram at 298 K and 1 atm. Compounds from left to right on the $CaO–SiO_2$ line are Ca_3SiO_5, Ca_2SiO_4, $Ca_8Si_5O_{18}$, $Ca_3Si_2O_7$, $CaSiO_3$, and $CaSi_2O_5$. $Ca_3Si_2O_7$ is not indicated on the diagram because its position is nearly indistinguishable from $Ca_8Si_5O_{18}$. $Ca_3Si_2O_7$ is also connected to Si by a tie line. The dashed tie line is somewhat uncertain, as discussed in the text.

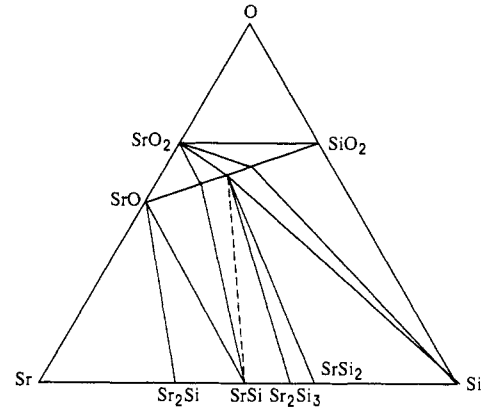

Figure 3. Sr–Si–O phase diagram at 298 K and 1 atm. Compounds from left to right on the $SrO–SiO_2$ line are Sr_3SiO_5, Sr_2SiO_4, and $SrSiO_3$. The dashed tie line is somewhat certain as discussed in the text.

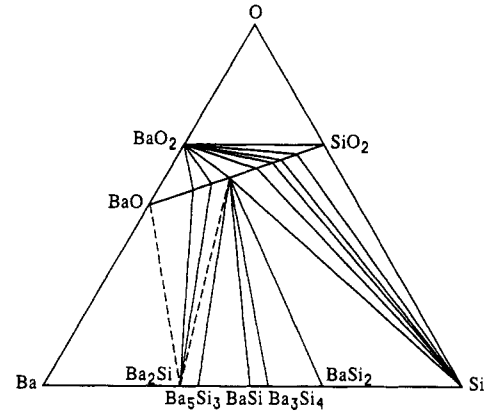

Figure 4. Ba–Si–O phase diagram at 298 K and 1 atm. Compounds from left to right on the $BaO–SiO_2$ line are Ba_4SiO_6, Ba_3SiO_5, Ba_2SiO_4, $BaSiO_3$, $Ba_2Si_3O_8$, $Ba_5Si_8O_{21}$, $Ba_3Si_5O_{13}$, $BaSi_2O_5$, and $BaSi_4O_9$. $Ba_5Si_8O_{21}$ and $Ba_3Si_5O_{13}$ are not indicated on the diagram because their compositions are nearly indistinguishable from $Ba_2Si_3O_8$ and $BaSi_2O_5$. Both compounds are connected to Si by tie lines. The dashed tie lines are somewhat uncertain, as discussed in the text.

because the known values of ΔH_f for calcium silicates compounds that have a similar composition are within 1.5% of the estimated values as shown in Table II. For the barium silicates, the estimated values for $Ba_5Si_8O_{21}$, $Ba_3Si_5O_{13}$, and $BaSi_4O_9$ should have relative errors of 0.8%. The values estimated for the silicides have much larger discrepancies with respect to the known values. The reasons for those differences are not known at present, although they may indicate that the uncertainties in the measurements are greater than the published error limits. Thus, the major limitations in the calculated phase diagrams result from the uncertainties in the ΔH_f values of the silicides.

In the Mg–Si–O system, all the data used for the calculations were taken from refs 9 and 11. The magnitude of the enthalpy changes for all the reactions used for determining the phase diagram in Figure 1 was more than 130 kJ, which is larger than the worst-case estimated uncertainty calculated for any of the reactions. There is a large range for ΔH_f reported in ref 20 for the Mg_2Si phase, but our calculations show that the phase diagram in Figure 1 is still valid for the entire range of values. In the Ca–Si–O system shown in Figure 2, the magnitude of the enthalpy changes for all the reactions are greater than 130 kJ except for the following reaction:

$$4CaO + 3CaSi_2 \rightarrow Ca_2SiO_4 + 5CaSi \qquad \Delta H = -69 \text{ kJ} \tag{1}$$

which has a smaller enthalpy change than the worst-case estimated uncertainty for this reaction, which is 107 kJ. Therefore, we used a dashed line in Figure 2 to connect Ca_2SiO_4 and CaSi to indicate the uncertainty of this tie line. In the Sr–Si–O system in Figure 3, nearly all the calculated reaction enthalpies had magnitudes larger than 119 kJ except for the following reactions:

$$4SrO + 3SrSi_2 \rightarrow Sr_2SiO_4 + 5SrSi \qquad \Delta H = -20.5 \text{ kJ} \tag{2}$$

$$4SrO + 3Sr_2Si_3 \rightarrow Sr_2SiO_4 + 8SrSi \qquad \Delta H = -55.0 \text{ kJ} \tag{3}$$

Thus, the tie line connecting Sr_2SiO_4 to SrSi is uncertain because the ΔH values for reactions 2 and 3 are relatively small in magnitude, so the tie line is shown dashed in the figure. In the Ba–Si–O system of Figure 4, the enthalpy changes for most of the reactions are more than the evaluated uncertainties in the enthalpy changes, with many of the values more than 500 kJ except for the following reactions:

$$Ba_2SiO_4 + 4Ba \rightarrow 4BaO + Ba_2Si \qquad \Delta H = -34.7 \text{ kJ} \tag{4}$$

$$4BaO + 4\,Ba_5Si_3 \rightarrow Ba_2SiO_4 + 11Ba_2Si \qquad \Delta H = -1.3 \text{ kJ} \tag{5}$$

Again, the BaO–Ba_2Si and Ba_2SiO_4–Ba_2Si tie lines are indicated by dashed lines.

The phase diagrams presented in Figures 1–4 were determined from the data tabulated in Tables I–IV, respectively, and calculations of all possible binary tie-line crossings. These phase diagrams were calculated from ΔH_f data at 298 K, but since the temperature dependence of the enthalpies is weak and should be roughly similar for all the oxide phases, the diagrams are probably correct over a range from 0 K to nearly the temperature of the lowest melting eutectic in each system. With the few exceptions noted above that are indicated by dashed lines, the positions of the tie lines in the diagrams are remarkably insensitive to uncertainties in the ΔH_f values.

We attempted to eliminate the uncertainties in the calculated phase diagrams by performing binary reaction experiments. Mixed powders of different phases were heated to 800 °C for 3 days in sealed quartz tubes. After the heating procedure, the resulting materials were examined by X-ray powder diffractometry. Unfortunately, it was not possible to identify the phases unambiguously, because of the large number of peaks in the diffraction patterns and the formation of large amounts of amorphous materials. Nevertheless, the phase diagrams presented here should represent the correct trends in the phase diagrams of these systems and thus should be of use to other researchers interested in these systems.

Discussion

The primary feature shared by all the diagrams in Figures 1–4 is that a series of ternary compounds, i.e., metal silicates, are intermediate in composition between the metal monoxide and silicon dioxide. These M–Si–O phase diagrams can be classified according to how elemental Si interacts with the various oxides: (1) the metal monoxide and all the metal silicates are connected to Si by a tie line (Mg–Si–O); (2) the metal monoxide is not connected to Si, but several metal silicates are (Ca–Si–O, Sr–Si–O, and Ba–Si–O).

Thus, elemental Si cannot reduce MgO or Mg silicates, whereas an excess of Si can reduce any of the oxides of Ca, Sr, and Ba to their respective disilicides. In the Ca–Si–O, Sr–Si–O, and Ba–Si–O systems, excess Si can react with Ca_3SiO_5, Sr_3SiO_5, Ba_4SiO_6, and Ba_3SiO_5 to form silicides and other silicates, but Si does not react with most of the silicates. On the other hand, in all cases excess elemental group II metals can reduce SiO_2 and all the silicates to silicides.

This type of information is extremely valuable if one wishes to evaluate the possibility of using different oxides as insulating layers on Si as alternatives to SiO_2. For example, Kado and Arita[25] reported on the growth of SrO films on Si. This system is of interest because SrO has a cubic crystal structure and is nearly lattice matched to Si. Thus, there was an intriguing possibility for growing heteroepitaxial structures. However, when Himpsel et al.[26] examined this system using photoemission, they found that SrO reacted with Si during the deposition to form Sr silicates. This observation is in agreement with the phase diagram in Figure 3, which furthermore predicts that Sr silicides should also have been formed in the reaction of SrO with Si. The actual products formed and their distribution on the Si substrate depends on the deposition and growth conditions (i.e., kinetic parameters), but if the system had been heated long enough to reach equilibrium, the deposited and reacted film would consist of a mixture of Sr_2SiO_4 and $SrSi_2$. Such films are clearly not desirable insulators, since the silicide is metallic, and thus if these phase diagrams had been available at the time, the experiments reported in ref 26 would not have been necessary.

Taking the opposite approach, one can examine the phase diagrams to determine what oxides involving group II metals are chemically stable with respect to Si. The list is MgO, Mg_2SiO_4, $MgSiO_3$, Ca_2SiO_4, $Ca_8Si_5O_{18}$, $Ca_3Si_2O_7$, $CaSiO_3$, $CaSi_2O_5$, Sr_2SiO_4, $SrSiO_3$, Ba_2SiO_4, $BaSiO_3$, $Ba_2Si_3O_8$, $BaSi_2O_5$, and $BaSi_4O_9$. Whether any of these phases would be of interest as insulators on Si depends on their structural and electrical properties, and significant amounts of research would be required to grow such films and evaluate their properties.

The phase diagrams in Figures 2–4 can also be used to estimate whether or not various forms of the new oxide superconductors are compatible with Si or SiO_2. Williams and Chaudhury[27] have analyzed the thermodynamic stability of the $YBa_2Cu_3O_7$ (YBCO) phase with respect to other materials and found that a good approximation of ΔH_f for YBCO is simply the sum of ΔH_f's for the component oxides. Both Si and SiO_2 react with YBCO to form more stable products, predominantly Ba silicates. However, they demonstrated that YBCO does not react with $BaSi_2O_5$, because of the extreme thermochemical stability of this compound.[27] On the basis of this information and the phase diagrams presented here, both Si and SiO_2 can also be ruled out as suitable substrates for either Ca- or Sr-containing oxide superconductors, but various other silicates may prove to be suitable as chemically inert substrates.

Several ternary oxides, such as $SrTiO_3$, $LaAlO_3$, and $LaGaO_3$, have been used with considerable success as substrates for growing highly oriented YBCO films.[28-30] These materials provide a good lattice match for the (001) planes of YBCO, and they appear to be chemically inert. This is most likely because these ternary oxides are also thermochemically very stable. An examination of the crystal structures of the group II metal silicates reveals that one high-temperature phase of Ca_2SiO_4 is trigonal with lattice constants a = 5.46 Å and c = 7.19 Å.[31] If this phase can be stabilized, it could also prove to be a reasonable substrate for YBCO. This material and other silicates are the subject of continuing investigations.

The major caveat to remember when applying these phase diagrams to real thin-film systems is that they are strictly valid only for closed systems with 1 atm of oxygen gas present. For systems that are examined in a vacuum or utilized in ambient conditions, gas-phase species such as SiO that may form on heating can escape and thus change the composition of a film from its as-deposited stoichiometry.[6] With this in mind, the ternary phase diagrams provided here should prove to be very useful for

(25) Kado, Y.; Arita, Y. *J. Appl. Phys.* **1987**, *61*, 2398.
(26) Himpsel, F. J.; Morar, J. F.; Yarmoff, J. A. *J. Electrochem. Soc.* **1988**, *135*, 2844.
(27) Williams, R. S.; Chaudhury, S. *Chemistry of High Temperature superconductors, II*; Nelson, D. L., George, T. F., Eds.; ACS Symposium Series; American Chemical Society: Washington, DC, 1988, Vol. 377; p 291.
(28) Wu, X. D.; Dijkkamp, D.; Ogale, S. B.; Inam, A.; Chase, E. W.; Miceli, P. F.; Chang, C. C.; Tarascon, J. M.; Venkatesan, T. *Appl. Phys. Lett.* **1987**, *51*, 861.
(29) Ecom, C. B.; Sun, J. Z.; Yamamoto, K.; Marshall, A. F.; Luther, K. E.; Geballe, T. H.; Laderman, S. S. *Appl. Phys. Lett.* **1989**, *55*, 595.
(30) Koren, G.; Gupta A.; Giess, E. A.; Segmuller, A.; Laibowitz, R. B. *Appl. Phys. Lett.* **1989**, *54*, 1054.
(31) Hellwege, K.-H.; Madelung, O. *Landolt-Bornstein Numerical Data and Functional Relations in Science and Technology*; Springer-Verlag: Berlin-Heidelberg, 1985; New Series, III/7d1.

designing thin film systems that incorporate the group II metals, silicon, and oxygen.

Summary

Ternary phase diagrams have been determined for the M-Si-O systems, where M = Mg, Ca, Sr, and Ba. These phase diagrams can be used to explain previous experimental results for reactions between SrO films on Si and to predict what can happen at the interfaces between M-containing compounds and either Si or SiO_2. These phase diagrams are not difficult to determine, yet they are important in providing guides in designing experiments and in selecting chemically stable materials for thin-film structures.

Acknowledgment. This work was supported in part by the Office of Naval Research. R.S.W. received partial support from the Camille and Henry Dreyfus Foundation.

Registry No. Mg, 7439-95-4; Ca, 7440-70-2; Sr, 7440-24-6; Ba, 7440-39-3; Si, 7440-21-3; O_2, 7782-44-7.

Use of Thiazole Rings To Enhance Molecular Second-Order Nonlinear Optical Susceptibilities

C. W. Dirk,*,† H. E. Katz, and M. L. Schilling

AT&T Bell Laboratories, 600 Mountain Avenue, Murray Hill, New Jersey 07974

L. A. King

AT&T Bell Laboratories, P.O. Box 900, Princeton, New Jersey 08540

Received July 25, 1990

It is shown that the appropriate replacement of benzene-ring structures by thiazole rings in polar donor-acceptor molecules will result in an increase of the microscopic scalar second-order nonlinear optical quantity, $\mu_0\beta$, of up to a factor of $\approx$3. Electric field induced second harmonic generation (EFISH) results are presented for two species of this type and compared to the corresponding benzenoid structures. In general, the results show the increases in $\mu_0\beta$ to be largely due to dispersion, with smaller effects seen in dipole and transition moments. There is a significant narrowing of the transition band from $2\Gamma \approx 3530$ cm^{-1} to $2\Gamma \approx 2110$ cm^{-1} upon replacement of benzene by thiazole, thus keeping the effects of damping relatively constant and permitting ready application of these dyes for electrooptic device applications in the near IR ($\gtrsim$1300 nm). Scalar $\mu_0\beta$ as large as $\approx$5300 D cm^5 esu^{-1} ($\lambda_{2\omega}$ = 789.5 nm; λ_{max} = 645 nm; Γ = 1057 cm^{-1}, the half-width at half-maximum) are observed for a (dicyanovinyl)thiazole azo dye.

Introduction

It is well-known that five-membered conjugated heterocycles (furan, thiophene, thiazole, etc.) possess considerably less aromatic stabilization than benzene, although they are considerably more stable than the acyclic butadiene analogues.[1,2] Thus, while the cost in energy to break the aromatic delocalization is less than in benzene, substantial thermodynamic stability remains. This observation is important for organic electronic and optical materials. Electrically conducting doped polythiophene[3] is a stable compromise between the air-unstable polyacetylene and the more poorly conducting polyphenylene analogues.[4] The relatively poor conductivity and greater stability of polyphenylene can be attributed to localization of electrons in each aromatic ring. Since the characteristics of nonlinear optical (NLO) materials depend on the intramolecular transfer of electron density, it could be argued that similar replacement of benzene moieties will lead to enhancements in the NLO susceptibilities. This will bring the susceptibilities closer to those of the donor-acceptor conjugated dienes, though the molecule will retain much of its stability and all of its planarity, and extended conformation, relative to those containing benzene rings. Zhao et al.[5] and independently Fichou et al.[6] have demonstrated large third-order susceptibilities, γ, in thiophene oligomers. Kaino et al.[7] have shown poly(2,5-thienylenevinylene) to possess a higher bulk third-order nonlinearity, $\chi^{(3)}$, than the phenylene analogue. Despite the promise of larger second-order nonlinearities in compounds containing heterocycles in place of benzene, there have apparently been no great successes reported in the literature for such compounds.

The second-order microscopic nonlinearity, β, is approximately given by a two-level model:[8]

$$\beta = K(\Delta\mu_{01})(\mu_{01})^2 F(\Omega_{01},\omega_1,\omega_2) \quad (1)$$

where K is a constant that depends on the optical process, μ_{01} is the scalar magnitude of the transition moment vector ($\int \Psi_0 e\mathbf{r}\Psi_1 \, d\tau$, where Ψ_0 and Ψ_1 are the ground- and excited-state wave functions, and $d\tau$ represents the integral over all space), $\Delta\mu_{01}$ is the change in dipole moment between the ground and first excited state (given by $\mu_{11}-\mu_{00}$),

† Present address: Department of Chemistry, University of Texas at El Paso, TX 79968-0513.

(1) Wheland, *Resonance in Organic Chemistry*; Wiley: New York, 1955; p 99.
(2) March, J. *Advanced Organic Chemistry*; 3rd ed.; Wiley: New York, 1985; pp 37-64.
(3) Kobayashi, M.; Chen, J.; Chung, T.-C.; Moraes, F.; Heeger, A. J.; Wudl, F. *Synth. Met.* **1984**, *9*, 77-86.
(4) Schacklette, L. W.; Eckhardt, H.; Chance, R. R.; Miller, G. G.; Ivory, D. M.; Baughman, R. H. *J. Chem. Phys.* **1980**, *73*, 4093-4102.
(5) Zhao, M.-T.; Singh, B. P.; Prasad, P. N. *J. Chem. Phys.* **1988**, *89*, 5535-5541.
(6) Fichou, D.; Garnier, F.; Charra, F.; Kajzar, F.; Messier, J. *Spec. Publ. R. Soc. Chem., Org. Mater. Non-linear Opt.* **1989**, *69*, 176-182.
(7) Kaino, T.; Kubodera K.; Kobayashi, H.; Kurihara, T.; Saito, S.; Tsutsui, T.; Tokito, S.; Murata, H. *Appl. Phys. Lett.* **1988**, *53*, 2002-2004.
(8) Oudar, J. L. *J. Chem. Phys.* **1977**, *67*, 446-457.

0897-4756/90/2802-0700$02.50/0